



PII: S0017-9310(96)00006-3

Pool boiling heat transfer on a thin plate: features revealed by liquid crystal thermography

D. B. R. KENNING and YOUYOU YAN

University of Oxford, Department of Engineering Science, Parks Road, Oxford OX1 3PJ, U.K.

(Received 20 April 1995 and in final form 18 December 1995)

Abstract—During pool nucleate boiling of water on a thin, electrically-heated plate, the motion of bubbles and the colourplay of a layer of thermochromic liquid crystal on the back of the plate were recorded simultaneously by a high-speed colour video camera at 200 frames/s. Quantitative conversion of the Hue component of the video signal to temperature provided information on the variations in wall superheat over an extensive region, on the mechanisms of heat transfer and on irregularities in the behaviour of nucleation sites. Copyright © 1996 Elsevier Science Ltd.

1. INTRODUCTION

The bubble-driven processes of heat removal in nucleate boiling are intrinsically unsteady and non-uniform. The amplitude of the consequent variations in wall temperature depends on the thickness and thermal properties of the heated wall. During pool boiling of water on the upper surface of a horizontal, electrically-heated stainless steel plate 0.13 mm thick, photographs of a coating of thermochromic liquid crystal on the lower surface of the plate showed that at any instant the spatial variations in wall superheat were large fractions of the mean superheat [1]. In subsequent experiments the colourplay of the liquid crystal was recorded by high-speed colour video camera at 200 frames/s [2, 3], revealing the variations in wall superheat during the growth and departure of individual bubbles. Preliminary analysis of these recordings was performed by Bergez [4], using 'eye-ball' conversion of liquid crystal colour to temperature. This paper describes the results of quantitative conversions of the Hue component of the video signal to temperature, followed by image analysis [5].

Despite some deficiencies in these exploratory experiments, analysis of the recordings reveals aspects of nucleate boiling at low heat flux that conflict with some well-established models for the mechanism of heat transfer and the conditions that determine the population of active nucleation sites. We show that the spatial variations in wall superheat must be included in any model, that the thermal disturbance caused by the growth and departure of a bubble is confined to the area under the bubble and does not extend to a larger 'area of influence', although convective cooling driven by the collective motion of bubbles may be significant, and we present examples of the irregular behaviour of nucleation sites and evidence of

interactions between sites that affect the population of active sites. The examples given in this paper are a small sample of the information contained in the recordings. They illustrate the advantages, and limitations, of liquid crystal thermography combined with high-speed colour video recording for the study of boiling heat transfer. The technique is necessarily limited to boiling on very thin walls, conditions that maximize the local variations in wall temperature and minimize lateral conduction. Results obtained under these conditions might be criticized as atypical of 'real' boiling. There may indeed be smaller variations in wall superheat during boiling on thick copper walls, but many industrial applications (and laboratory experiments) involve boiling on materials of low thermal conductivity ranging from stainless steel to coated glass. We see the role of experiments with liquid crystal on thin walls as the identification of mechanisms and the testing, under these special conditions, of models for nucleation site behaviour and heat transfer near bubbles that can then be applied in large-scale numerical models, such as that developed at Los Alamos National Laboratory [6, 7], that are capable of modelling the interactions between many nucleation sites on thick walls.

2. EXPERIMENTAL METHODS

The heater was a stainless steel plate 28.1 × 40.8 mm and 0.13 mm thick, sealed at its edges by silicone rubber over an aperture in the bottom of a glass-sided tank 46 × 103 mm in cross-section and 100 mm deep. The plate was heated by the passage of ripple-free direct current from a rotary generator, fed through heavy brass electrodes soldered to the pool side of the plate. The tank was filled with water that had been degassed by boiling in a separate vessel, but, because

NOMENCLATURE

a	microlayer thickness [m]	Greek symbols	
b	$(\rho_1 c_1)/(\rho_s c_s \delta)$ [m^{-1}]	α	thermal diffusivity [$\text{m}^2 \text{s}^{-1}$]
c	specific heat [$\text{W kg}^{-1} \text{K}^{-1}$]	δ	wall thickness [m]
h	heat transfer coefficient [$\text{W m}^{-2} \text{K}^{-1}$]	ν	kinematic viscosity [$\text{m}^2 \text{s}^{-1}$]
k	thermal conductivity [$\text{W m}^{-1} \text{K}^{-1}$]	ρ	density [kg m^{-3}].
q	heat flux [W m^{-2}]	Subscripts	
q_0	input heat flux [W m^{-2}]	b	bulk liquid
t	time [s]	l	liquid
T	temperature [°C]	m	maximum
ΔT_s	superheat [K]	s	solid
x, y	coordinates in plane of wall [m]	w	wall.
z	coordinate normal to wall [m].		

the tank was open to the atmosphere, the gas content of the water pool was not completely controlled. Two series of experiments were performed on the same plate, one with the plate poorly-wetted with a contact angle exceeding 50° and the other with the plate well-wetted with a contact angle of less than 20° . The contact angles were not measured accurately. The poorly-wetted condition was produced by cleaning with acetone, rinsing with water and then allowing the plate to dry before immersion in the boiling pool. The well-wetted condition was produced by scrubbing with a residue-free detergent followed by prolonged rinsing with hot tap water and then demineralized water; the surface was then coated with a wet tissue until the moment of immersion.

The underside of the stainless steel plate was coated with a thin layer of black paint, then a layer of unencapsulated thermochromic liquid crystal approximately 0.010 mm thick and finally a protective layer of polyester film 0.025 mm thick. The liquid crystal had a visual colourplay range from 104°C (red start) to 123°C (green/melt). The colourplay on the underside of the plate and the bubble activity on its topside were recorded simultaneously at 200 frames/s by a NAC 200 colour video camera. Illumination was provided by a xenon flash tube, flash duration 20 μs , synchronized with the camera. Each video frame carried a time label, a normal view of the liquid crystal in the lower half of the frame and an oblique view of the bubbles at an angle of 30° from the horizontal in the upper half of the frame, Fig. 1. The oblique view was chosen as a compromise to provide a good indication of the instant of detachment of bubbles and sufficient indication of their front-to-rear position on the plate for matching with changes in the image of the liquid crystal.

The NAC 200 camera system recorded for up to 20 min at 200 frames/s in NTSC format on VHS video tape. Alternate pairs of frames were interlaced, each using half the total number of 525 camera lines. The camera provided playback of individual frames on an integral PAL monitor with slow/freeze/reverse facili-

ties. We had occasional use of a NAC 400 system with a NTSC or PAL external output, but generally analysis of the recordings had to be performed when the cameras were not available, so the original NTSC recordings were played back on a conventional machine that replayed each pair of interlaced frames simultaneously. The video signal was fed to a personal computer through a RGB decoder and a Data Translation 2871 frame grabber with on-board conversion to HSI (Hue-Saturation-Intensity) variables. The computer controlled the selection of sequences of up to 300 frames, an area of 128×162 pixels to be recorded from each frame and the signal components (Hue for the liquid crystal region and Intensity for the measurement of bubbles) to be stored on the hard disk of the computer. The software operations separated the interlaced frames, applied a Hue-temperature conversion derived from calibration experiments and performed image-processing operations such as filtering, averaging and contour-plotting.

The Hue-temperature relationship changes slowly with time, particularly if the liquid crystal is exposed to u.v. light, and depends on the angles of lighting and viewing as well as the settings of the camera and the decoder. Consequently it is highly desirable to calibrate the liquid crystal *in situ*, with the heat transfer surface at uniform, known temperatures. This was difficult in these experiments because of the simple, open construction of the tank. The water in the tank could not be pressurized to achieve temperatures up to 123°C without boiling, and immersion in a high-boiling liquid like silicone oil would have contaminated the system, which was therefore calibrated dry. A brass block with an embedded thermocouple was placed at the centre of the test surface inside the tank. Hot air was blown into the tank at high speed. Its temperature was increased gradually from a value just below the start of the colourplay of the liquid crystal and video recordings were made at intervals of 2 K. Heating was stopped just below the melting point of the liquid crystal and recordings were repeated as the test section was slowly cooled back through the

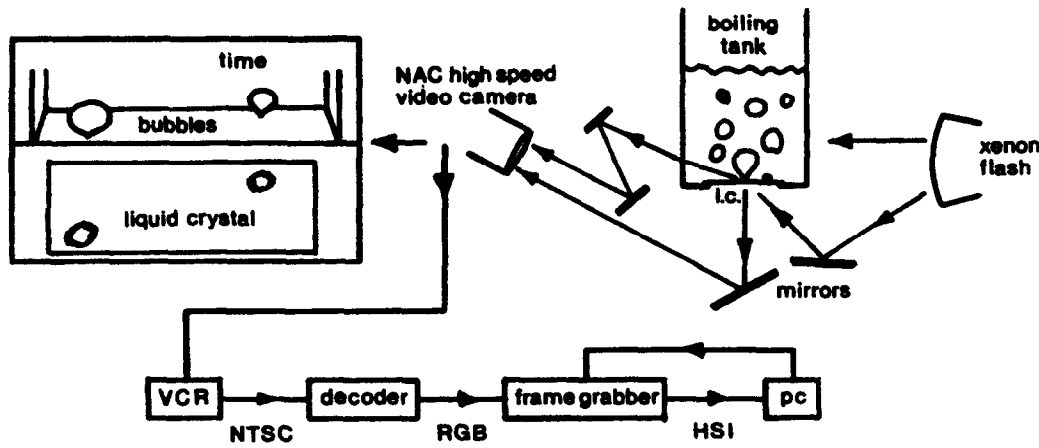


Fig. 1. Pool boiling experiment and analysis systems.

colourplay range. The Hue-temperature calibration was nonlinear, Fig. 2, and could be modified slightly by adjustment of the RGB decoder. There was a systematic difference between the heating and cooling calibrations, probably caused by the heating and cooling rates being too fast for complete equilibration of temperature between the test surface and the brass block containing the thermocouple. Later experiments on samples of liquid crystals with better thermal control did not exhibit this hysteresis. For the experiments discussed here the systematic uncertainty in wall superheat due to the deficiencies in the calibration procedure is about ± 1 K. (Financial constraints have so far prevented repetition of the pool boiling experiments with improved procedures.) There is also random high-frequency noise that particularly affects the accuracy of calculations of heat flux from the time-derivative of temperature during the rapid transients associated with the growth and departure of bubbles. These events occur within four or five video frames so that filtering in the time domain is not possible. The noise appears to originate mainly in the replay/data-capture system, since it is different on repeated replays of the same sequence of frames. Its amplitude is equivalent to ± 0.3 and ± 0.4 K at the top and bottom of the temperature range, but increases locally to ± 1.1 K around $108\text{--}110^\circ\text{C}$. Spatial averaging reduces the

noise at the cost of spatial resolution. Without averaging, the horizontal (x) resolution is limited by the camera resolution, equivalent to 0.25 mm. For this study a combination of spatial averaging over 3×3 pixels and ensemble averaging over 10 replays reduces the effect of noise to below ± 0.1 K over most of the range and to ± 0.3 K around $108\text{--}110^\circ\text{C}$. Further work is required to reduce the effect of signal noise and to improve the inversion of the temperature data for the rear, adiabatic surface of the plate to give the temperature and heat flux fields at the front boiling surface. The time constants δ^2/α for the 0.13 mm thick stainless steel and the 0.01 mm thick liquid crystal are 4 and 1 ms respectively, introducing a delay approximately equal to the period between video frames. No allowance for this delay has been made in the calculations that follow in Section 5.

Liquid crystal thermography applied to boiling has a lower frequency response and is less accurate than surface temperature measurement by micro thermocouples, e.g. [8], or resistance thermometers, e.g. [9]. Its advantages are the extensive nature of the measurements compared to a few spot measurements and the absence of disturbance to the microgeometry and wettability of the boiling surface.

3. EFFECT OF SURFACE WETTABILITY ON BOILING

Two series of experiments were performed, firstly with the stainless steel plate in the poorly-wetted condition and then in the well-wetted condition. The same plate was used, so there was no change in the microgeometry of the surface. The heat flux was increased at intervals of 1 min in steps of 25 kW m^{-2} from 50 kW m^{-2} to 150 kW m^{-2} (poorly-wetted) or 225 kW m^{-2} (well-wetted) then back to 100 , 75 , 50 kW m^{-2} with the camera running continuously. The bulk liquid temperature was 94°C at 50 kW m^{-2} , rising to 98°C at 75 kW m^{-2} and 100°C at higher fluxes. Comparative video pictures for the two conditions of the surface are shown in Fig. 3.

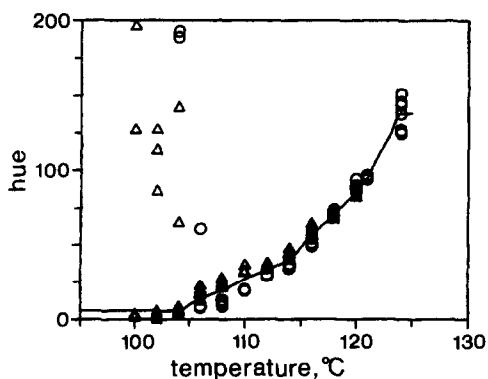


Fig. 2. Hue-temperature calibration.

The poorly-wetted surface is crowded with small bubbles even at a low heat flux of 75 kW m^{-2} . The bubble frequencies are too high for the liquid crystal to follow the variations in wall temperature caused by individual bubbles, but a flickering effect can be seen at some sites. There are small-scale spatial variations in the wall temperature between 106 and 116°C . With increasing heat flux, the wall temperature becomes more uniform through the elimination of hot spots; the increase in bubble production obscures the viewing of bubble motion near the wall.

When the surface is well-wetted, there are only a few bubbles visible at any instant at 75 kW m^{-2} . (There are some small, near-stationary bubbles at the joint between the stainless steel plate and the silicone rubber seal in the extreme foreground and background.) Some nucleation sites produce large bubbles at low frequencies; others produce smaller bubbles at higher frequencies and some sites produce the occasional small bubble. The growth of the bubble causes a cold (red) spot surrounded by a hotter (green) region; the cold spots persist long after bubbles have departed. At 100 kW m^{-2} , it is still just possible to follow the growth of some individual bubbles. At higher fluxes the cloud of bubbles obscures the view of the surface, but the cold spots characteristic of the formation of individual bubbles can still be seen on the liquid crystal on the back of the plate.

For both conditions of the surface, the rising bubbles drive an asymmetrical circulation of the liquid in the tank, with a stronger flow down the front wall than down the back wall. This flow causes convective cooling, most clearly seen on the well-wetted surface in Fig. 3 as a red region spreading in from the front edge at 150 kW m^{-2} and on both edges at 200 kW m^{-2} . The column of rising bubbles pulsates at low frequency and a corresponding fluctuation can be detected in the convectively cooled regions. The observations run counter to the conventional assumption that the contribution of convection to the total heat flow in nucleate boiling decreases as the heat flux increases. The effect is likely to be sensitive to the geometry of the boiling system.

Changing the wettability of a surface of fixed micro-geometry completely changed the nature of the boiling process and of the accompanying variations in wall temperature. On the poorly-wetted plate the small-scale, high-frequency variations cannot be resolved properly in these recordings. This might be overcome by taking pictures at higher magnification, which would restrict the field, and by using a thinner plate made of a material of higher thermal conductivity. The larger-scale, slower events on the well-wetted plate can be resolved and the remainder of the paper is restricted to this condition.

4. DISTRIBUTIONS OF WALL SUPERHEAT

Experimental boiling heat transfer data are conventionally presented as a relationship between heat

flux and wall superheat in which both quantities are implicit space-time average values at the fluid–solid interface. The temperatures recorded on the back of the well-wetted plate at heat fluxes of 50 , 100 , 150 and 200 kW m^{-2} have been analysed over an area $20 \times 11 \text{ mm}$ and a period of 12 s , using 162×64 pixels from alternate video frames at intervals of 0.01 s (1200 time samples, 12×10^6 samples in all). No correction has been made for the temperature difference between the back and the front of the plate, which increases from 0.2 K at 50 kW m^{-2} to 0.8 K at 200 kW m^{-2} . The average values and distributions of superheat at each heat flux are plotted in Fig. 4, together with the spatial distributions of time-averaged superheat (the time-averaged reading that would be registered by a local thermometer). The average superheat varies with heat flux by only 1.6 K , from 13.7 K at 50 kW m^{-2} through a maximum of 15.3 K at 100 kW m^{-2} and back to 14.0 K at 200 kW m^{-2} . The distributions of superheat do not change much with heat flux either, ranging between 6 and 20 K at 50 kW m^{-2} and between 4 and 22 K at higher fluxes. With such wide ranges, it is clear that models for bubble nucleation and growth that assume uniformity of wall superheat cannot be realistic. The spatial distributions of time-averaged superheat do change with heat flux. Some of the smaller-scale features present at low flux are smoothed out at high flux and the convective cooling spreading in from the front edge of the plate contributes to the reduction in average superheat. These distributions show that conventional methods of measuring wall superheat in this sort of experiment by an array of four to six small thermocouples attached to the back of the plate could lead to large errors in the measurement of average wall superheat [1].

5. THERMAL CONSEQUENCES OF BUBBLE GROWTH

This section refers entirely to boiling on the well-wetted plate at the lowest heat flux of 50.8 kW m^{-2} , when there is a clear view of the motion of individual bubbles. The bulk liquid is 6 K subcooled.

First we examine the changes in wall temperature during the growth and departure of a large bubble. A1. at site A. The distributions of wall superheat (on the back of the plate) at temperature intervals of 2 K and time intervals of 5 ms are shown in Fig. 5. The marked position of the nucleation site is the centroid of the thermal disturbance during the early stages of bubble growth. The superimposed circles show the horizontal diameter (dotted line) and apparent contact diameter (solid line) found from Intensity measurements on the oblique view of the bubble and assuming circular symmetry. The contact region may be distorted by the gradient of refractive index near the wall [10]. There is an uncertainty of $\pm 0.13 \text{ mm}$ in the relative horizontal positions of images of bubbles captured in the upper half of the frame and the image of the liquid crystal below. The bubble nucleates at

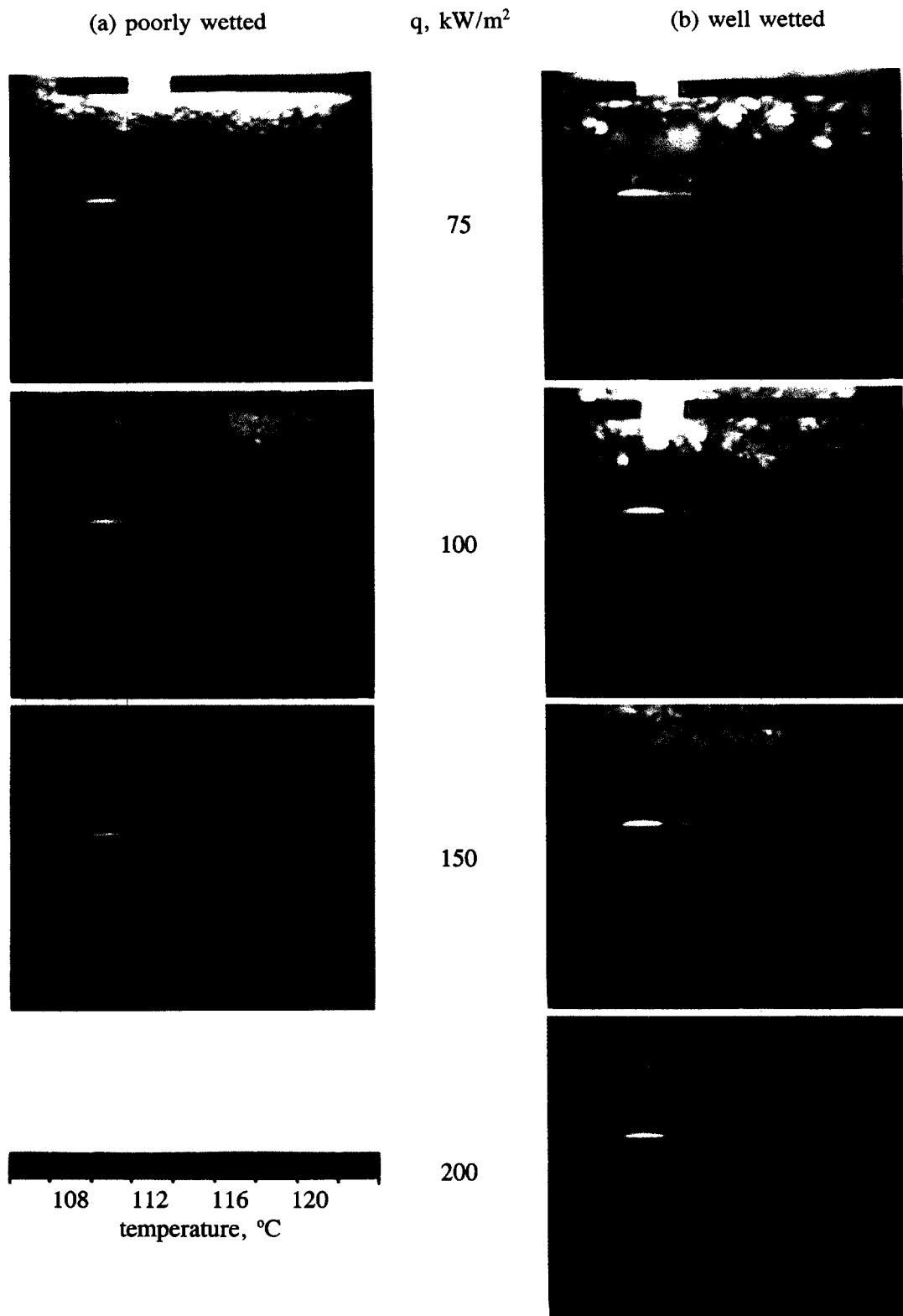


Fig. 3. Video frames : (a) poorly-wetted surface, (b) well-wetted surface.

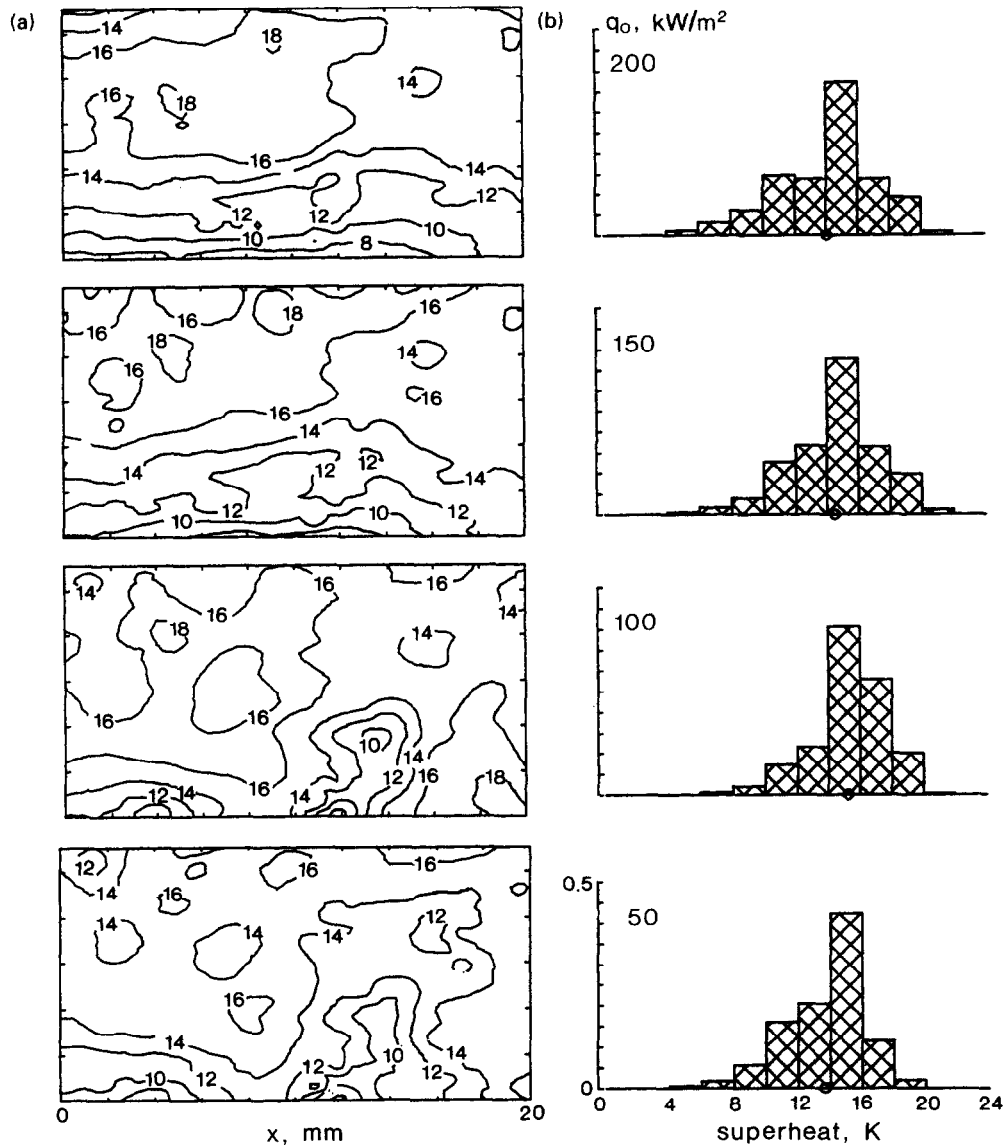


Fig. 4. Distributions of wall superheat: (a) contours of time-averaged superheat, (b) histograms.

some time between 07.045 and 07.050 s, when the temperature at the nucleation site is 115.7°C. At 07.060 it reaches its maximum diameter of 5.5 mm, with a contact diameter of approximately 4.4 mm. Then the bubble starts to round off: the horizontal diameter decreases slightly and the contact diameter decreases until the bubble detaches just before 07.070. At 07.075 the bottom of the bubble is about 2.2 mm above the plate and at 07.080 it is out of sight, at least 6 mm above the plate. Because the bubble is viewed obliquely, it is not possible to determine its true profile and hence, its volume.

In frames 07.040 and 07.045 immediately before nucleation, the wall superheat is nonuniform and is evolving slowly with time. Following nucleation, it is difficult to detect the influence of the bubble in Fig. 5 until a cooled, roughly circular region appears at

07.060. This region increases in size and at 07.070, just after bubble detachment, it matches approximately the maximum area of contact that occurred at 07.060. After detachment, the cooled footprint slowly warms up again during a recovery period that lasts typically 200 ms. The influence of the bubble is better seen by subtracting from the initial temperature field at 07.040 the temperature fields at subsequent times, Fig. 6. The contours, now plotted at intervals of 1 K, show the decreases in temperature. They confirm that the cooled region lies within the maximum projected area of the bubble at time 07.060 and that it does not spread much during the recovery period after bubble detachment. Contrary to a popular modelling assumption [11], the thermal 'area of influence' of the bubble is not bigger than the bubble itself.

The temperature profiles on a line through

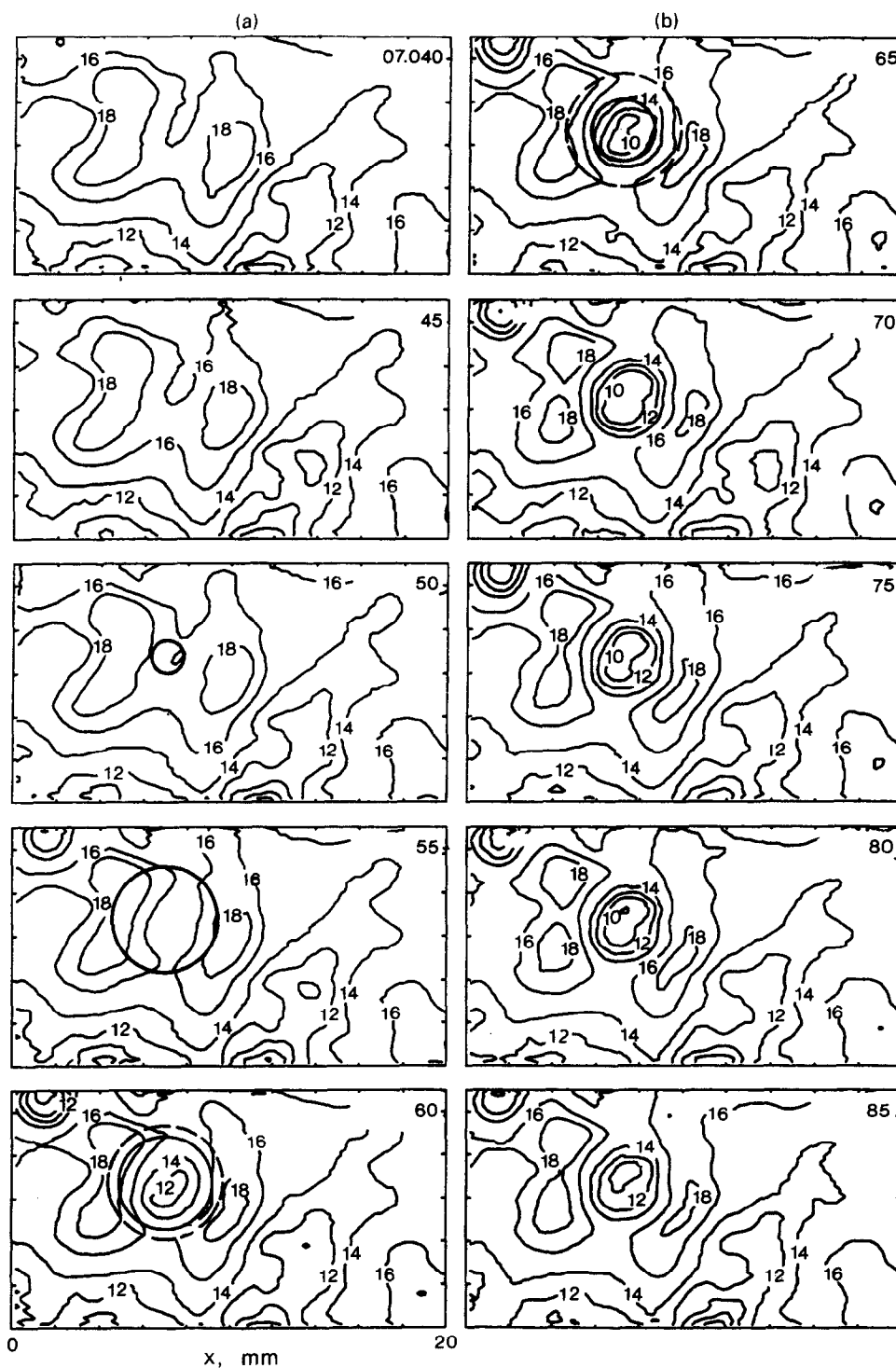


Fig. 5. Variations in wall superheat, bubble A1.

nucleation site A, the positions of the bubble perimeter and of the apparent contact line with the wall (with an indication of the uncertainty of position relative to the nucleation site) and the calculated distributions of surface heat flux are shown in Fig. 7 for bubble A1 and for a later bubble A2. Bubble A2 nucleates at the same superheat at A1, but the initial distribution of wall superheat round the nucleation site is much less

symmetrical and the bubble has a slightly smaller maximum diameter. As noted in Section 2, the calculation of heat flux is at present unrefined. Neglect of the time required for temperature changes to diffuse through the thickness of the plate introduces a delay of about 5 ms (one video frame) between the position of the bubble boundary and the temperature and heat flux fields. Lateral diffusion in the plate is included

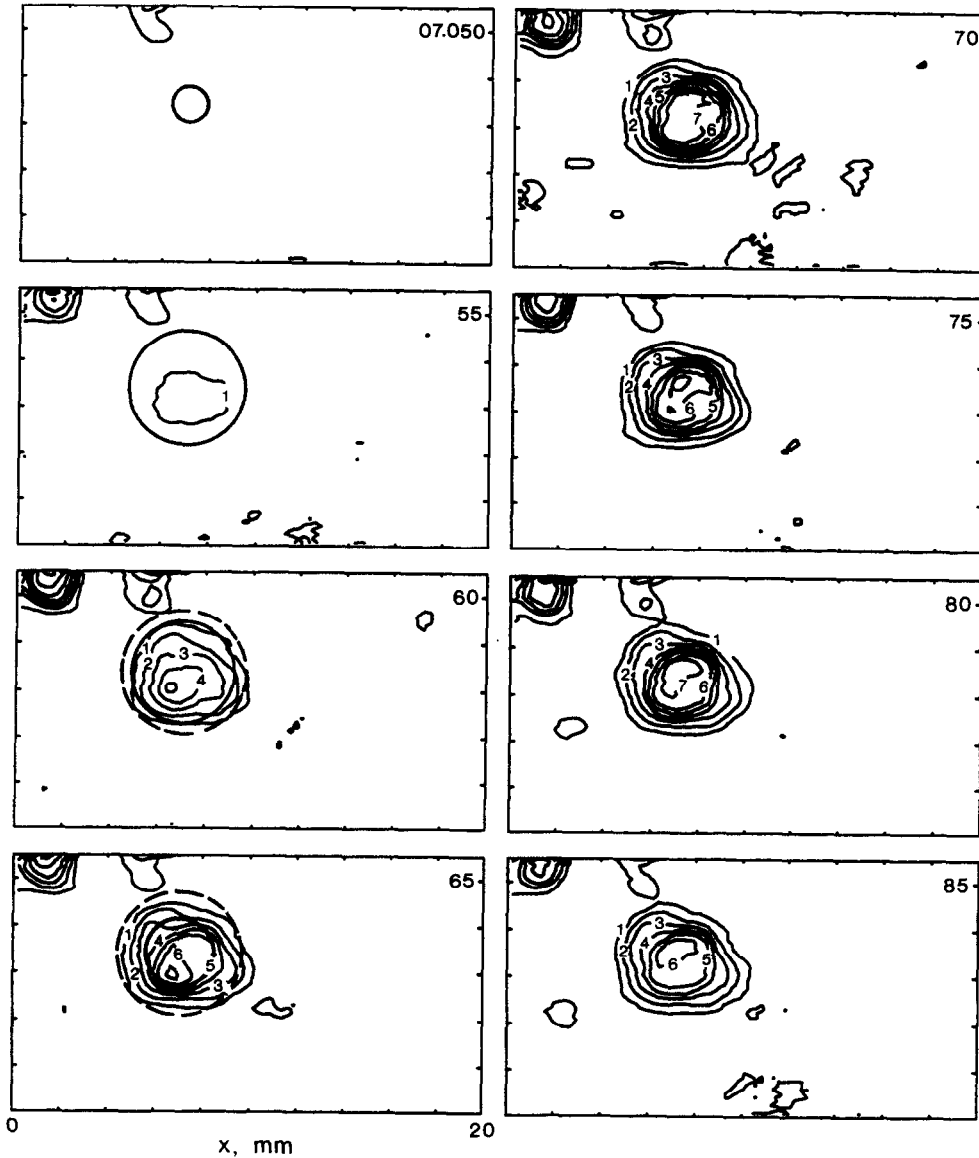


Fig. 6. Decreases in wall superheat, bubble A1.

in the calculation so the surface heat flux q is found from

$$q = q_0 + k_s \delta \left(\frac{\partial^2 T}{\partial x^2} + \frac{\partial^2 T}{\partial y^2} \right) - \rho_s c_s \delta \frac{\partial T}{\partial t}. \quad (1)$$

Signal noise of amplitude 0.3 K, which may be present at the lower superheats that are developed under the bubble, can generate errors of about 25 kW m^{-2} in the calculations of heat flux during the rapid growth and departure of the bubble, comparable with the steady input heat flux q_0 of 50.8 kW m^{-2} . (During the recovery period the changes are much slower and smoothing in the time domain can be used.)

During the growth of bubble A1 to its maximum size at 07.060, over a growth time $t_m \sim 12 \text{ ms}$, the region of high wall heat flux coincides (within the space-time uncertainty) with the projected area under

the bubble, Fig. 7(a). At 07.060, the heat flux rises from the background level at the perimeter to a maximum of about 300 kW m^{-2} near the centre of the bubble, with a slight dip right at the centre. During the growth of the bubble it is expected that a liquid microlayer will be formed under the contact region of the bubble with maximum thickness a_m at the perimeter of order $0.8 (v_l t_m)^{1/2}$ [12], equal to 48 microns in this case, decreasing approximately linearly to zero at the nucleation site. The quasi-steady heat flux through a microlayer of local thickness a for local wall superheat ΔT_s is

$$q = \frac{k_l \Delta T_s}{a}, \quad (2)$$

but, except near the centre, the heat flux at the liquid-wall interface will be reduced because of the time taken

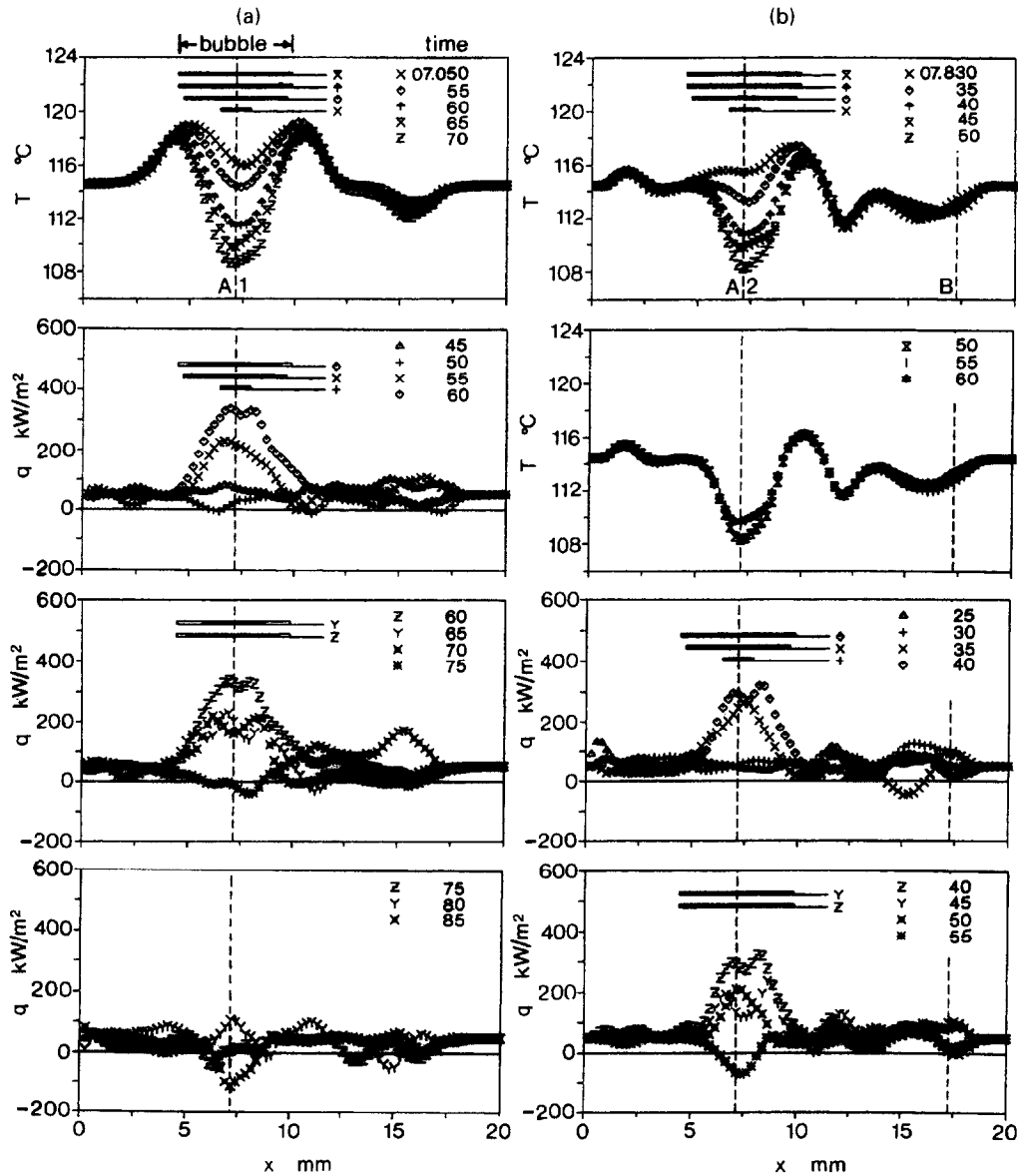


Fig. 7. Radial distributions of wall temperature and heat flux: (a) bubble A1, (b) bubbles A2, B1.

to establish the temperature gradient through the microlayer. Consider, for example, the microlayer at a radius of 1.1 mm with an estimated initial thickness a of 24 microns. The thermal diffusion time constant (a^2/α_1) is 3.4 ms, which is not small compared to the lifetime of the microlayer of about 10 ms up to 07.060. Then the local superheat is 14 K and the heat flux calculated from the experimental observations by equation (1) is 290 kW m⁻², compared to 400 kW m⁻² calculated by equation (2). The decrease in heat flux at larger radii in Fig. 7(a) is consistent with the increased effect of transient conduction across the regions of the microlayer with greater thickness and shorter lifetime. There appears to be a region of slightly enhanced heat transfer beyond the edge of the contact area up to the projected edge of the bubble, so there may be some small effect of convection in the

region of high curvature of the growing bubble, just beyond the edge of the microlayer. As the contact area decreases towards zero at 07.070, an elevated rate of heat transfer is maintained over the area originally covered by the bubble. This is consistent with convective cooling by bulk liquid flowing in under the bubble as it rounds off; the heat flux is well below the level predicted by the conventional quenching model that assumes instantaneous contact between the wall and liquid at the subcooled bulk temperature (Appendix A).

The heat transfer near the centre of the bubble over the period 07.050–07.065 is not consistent with the conventional model of microlayer formation with negligible thickness near the nucleation site. The initial heat fluxes round the site should be very high, causing rapid dryout (and then the cessation of heat transfer)

over a very small central region. The central heat fluxes at 07.060 and 07.065 are actually not much bigger than the fluxes at a radius of 1.1 mm and the corresponding thicknesses of the microlayer deduced from equation (2) are 24 and 33 microns, respectively, although evaporation should cause a decrease in thickness with time. (At 07.070, it is unclear whether cooling at the centre is the last stage of microlayer evaporation or the commencement of convective cooling by the bulk liquid.) The sustained cooling until at least 07.065 indicates that liquid is still present very close to the nucleation site. The microlayer formed during the very early stages of bubble growth may be thicker than is generally supposed. Alternatively, if a small dry patch is formed, surface tension forces may redistribute the microlayer in a way that causes the apparent increase in thickness between 07.060 and 07.065; intense evaporation at the contact line [13, 14], too localized to be resolved in these experiments, may also contribute to cooling. During the contraction of the contact area, which cannot be observed accurately, there may be a mechanism that feeds liquid from the periphery towards the centre of the microlayer.

At 07.075, when the bottom of the bubble is 2.2 mm above the plate, the heat flux has become very small everywhere across the projected area originally covered by the bubble. It even goes negative in one small region, implying contact with highly superheated liquid, but the calculations of heat flux are unreliable at such low values because of signal noise. At 07.080 there is a temporary increase in heat flux, too large to be an artefact of noise, over an area of diameter 3.4 mm, with a local minimum at that diameter and slightly higher fluxes beyond it. By 07.085 the heat flux has reverted to low values, some negative, everywhere in the footprint of the bubble. The short-lived heat removal at 07.080 may be caused by the wake flow behind the departing bubble, or by nucleation of a small subsidiary bubble undetected by the video camera, which samples an illuminated period of 20 μ s in every 5 ms. Small single bubbles appearing in a single video frame have been identified as the cause of similar localized disturbances, such as the one centred on $x = 15$ mm in Fig. 7(a) at 07.070.

Bubble A2 exhibits the same general behaviour as bubble A1 during growth, Fig. 7(b). There are some differences during departure that may be genuine or may result from the attempt to resolve rapid events with a camera speed of only 200 frames/s. The disturbances caused by a bubble at site B, which produces smaller bubbles at higher frequency than site A, are shown at the right hand side of Fig. 7(b). This bubble grows and departs over only three video frames so that analysis is inaccurate. Nevertheless, it shows that for this bubble, as for bubbles A1 and A2 and all other bubbles so far examined, the thermal disturbances during growth and departure are confined to the maximum projected area of the bubbles.

The rapid events of growth and departure are fol-

lowed by the gradual recovery of wall superheat leading to nucleation of the next bubble. As the bubble is well clear of the wall, the heat transfer data are presented as plots of the heat transfer coefficient $h(x, y, t)$ between the wall and the subcooled bulk liquid

$$h = \frac{q}{T_w - T_b}, \quad (3)$$

where q is calculated from equation (1). In order to reduce the effects of signal noise at the low heat fluxes during recovery, temperatures are averaged over 3×5 pixels and the time step is increased to 20 ms. During the recovery period following bubble A1, there is a persisting distribution of h around A, on which are imposed small-scale variations, Fig. 8(a). The area of the wall originally covered by the bubble is subjected to a heat transfer coefficient fluctuating in the range 1.7–2.3 $\text{kW m}^{-2} \text{K}^{-1}$. The recovery is interrupted after 100 ms by the growth of a bubble from an adjacent site that cools the region around A. The recovery after bubble A2 is not interrupted. Again there is a slowly-evolving general distribution of h with small-scale variations between 1.7 and 2.6 $\text{kW m}^{-2} \text{K}^{-1}$, Fig. 8(b). The variations are not symmetrical about A, so it is unlikely that they are caused by the wake behind the bubble rising from A, and there is no obvious influence from the nucleation of bubbles at sites at least 5 mm (about one bubble diameter) from A. Therefore it is likely that the convective heat transfer during recovery is driven by the circulation in the boiling cell and/or the local collective motion of bubbles. At A the coefficient of heat transfer is about 2.5 times the value of 840 $\text{W m}^{-2} \text{K}^{-1}$ calculated for natural convection at a temperature difference of 20 K (14 K average wall superheat plus 6 K subcooling); we have not yet examined its value at all points on the boiling surface.

In this section we have examined in detail examples of the growth of 'isolated' bubbles uninfluenced by other bubbles, except through their contribution to the nonuniformity of the superheat of the wall at the instant of nucleation. The bubbles grow at high superheat, at Jacob numbers of about 50, which would not be typical of boiling at high pressures. Growth and departure occur rapidly in tens of milliseconds, so the liquid crystal technique has been stretched to its limits in these experiments: optimization of conditions should improve the resolution of the relative timing of motion of the bubble boundary and heat transfer from the wall. The bubbles grow on a thin wall that changes temperature significantly as a consequence of heat transfer and this may alter the relative importance of different mechanisms. For example, it imposes a long waiting time between bubbles, so there can be no cooperative hydrodynamic effect of bubbles leaving the same site in quick succession. All these conditions must be kept in mind because there has often been a tendency in boiling research to apply too widely conclusions based on special conditions.

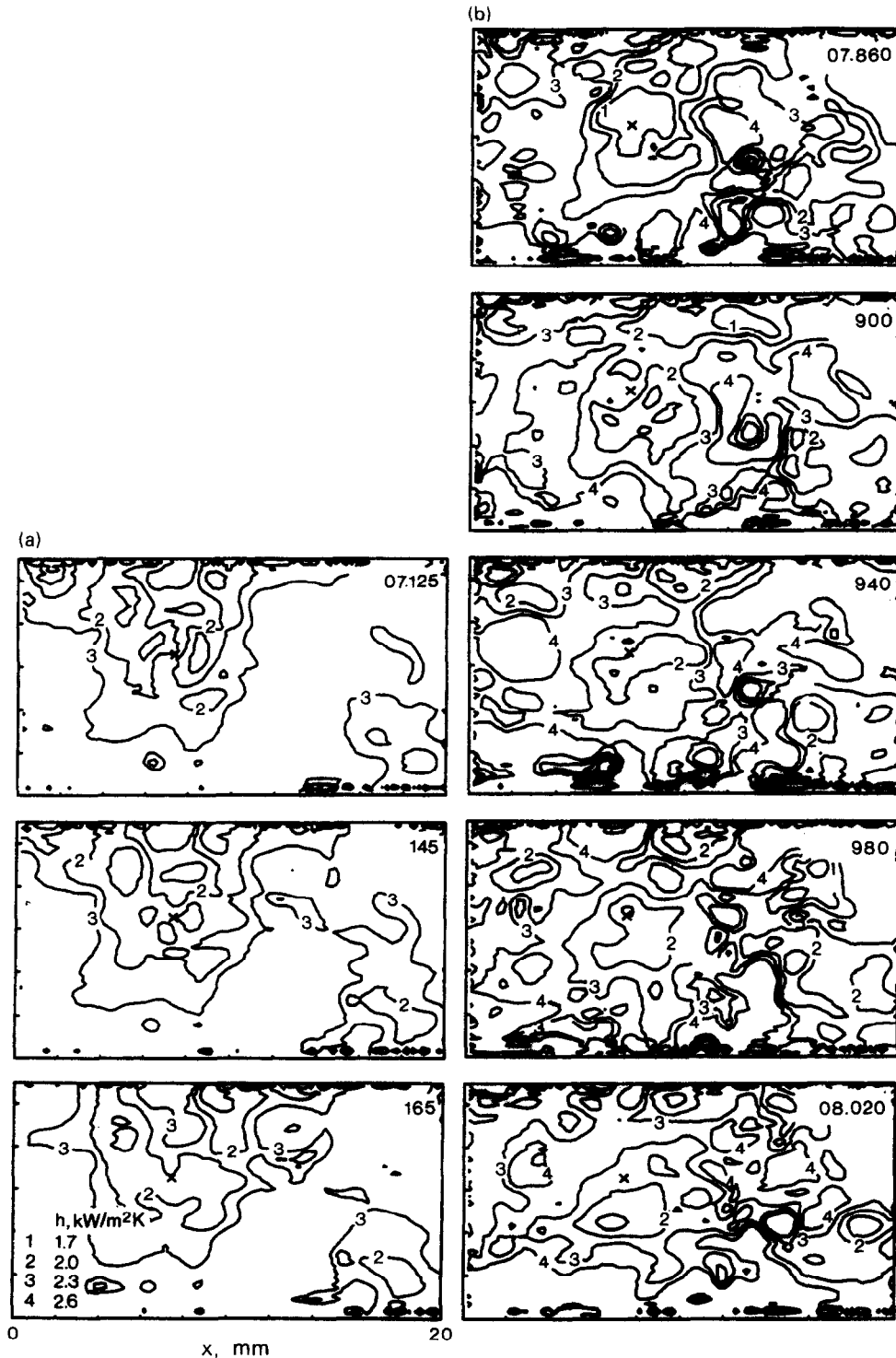


Fig. 8. Distributions of heat transfer coefficient following bubble departure, (a) bubble A1, (b) bubble A2.

Nevertheless, there are some indicators of general behaviour that can be identified from these experiments:

(i) *Microlayer evaporation*

This is an important mechanism of heat transfer, confined to the contact area between the bubble and

the wall. Current theories give the right order of magnitude. Calculations of the evaporation rate should include the initial nonuniformity of wall superheat round the nucleation site, which is one source of variability and asymmetry in the growth of bubbles from any site. Further consideration is required of the early stages of microlayer formation near the nucleation

site: the contribution by this small area to the total heat flow into a bubble may not be large, but the cooling of the site and the subsequent recovery to the nucleation superheat determine the frequency of bubble production.

(ii) *Wall quenching by bulk liquid*

As the bubble contact area contracts towards zero at lift-off, there appears to be heat transfer to liquid moving in towards the wall behind the retreating interface. This heat transfer does not extend beyond the maximum projected area of the bubble on the wall. This should not come as a surprise: the long series of studies by Cooper and colleagues of bubble growth under a variety of idealized conditions, e.g. [12, 15], did not detect any variations in wall temperature outside the projected area of the bubble. The heat flux is low at the perimeter of the bubble, increasing towards its centre. It is reduced by the precooling of the wall by microlayer evaporation but, even allowing for this and for the finite thermal capacity of the thin wall, its magnitude is well below that predicted by transient conduction in the bulk liquid following instantaneous contact with the wall. The wall-quenching model [11], with its twin assumptions of uniform transient conduction from an area of influence with radius about twice the maximum bubble radius, is clearly unrealistic for the conditions of these experiments. Consequently variants of the model applied to boiling under other conditions, e.g. Judd and Lavdas [16] for pool boiling on a glass and del Valle and Kenning [17] for subcooled flow boiling on a thin stainless steel wall, in which areas of influence much bigger than the bubble projected area are used to reconcile theory and experiment, must be regarded with suspicion unless direct evidence can be obtained for the occurrence of high rates of heat transfer outside the bubble projected areas under those particular conditions.

(iii) *Convective cooling by bulk liquid*

Conventionally this has been assumed to operate only outside the bubble areas of influence and has been calculated from correlations for the single phase heat transfer coefficient in the absence of boiling, e.g. [16]. In these experiments convective cooling occurred over the bubble area, starting just after bubble departure and continuing through the period of superheat recovery at a fluctuating rate about 2.5 times the rate for single phase natural convection. We do not know how to calculate the convective rate, but expect it to depend on some integrated effect of the bubble production, perhaps from a group of sites. It is a significant contributor to the total heat transfer because of the long recovery times between bubbles; it might be less important in conditions that give short recovery times. In Section 3 we noted that convection may increase in importance at higher heat fluxes, depending on the bubble-driven circulation in the boiling tank. The role of convective cooling in pool boiling requires further examination.

6. NUCLEATION SITE BEHAVIOUR

The near-circular patterns of temperature change under growing bubbles provided a means of identifying nucleation sites. Over a period of 12 s at a heat flux of 50.8 kW m^{-2} the Hue values for video fields at intervals of 10 ms were subtracted from those for the preceding field. Each resulting field was scanned, by a standard image-processing routine, to identify near-circular regions of diameter exceeding 1.3 mm and a decrease in Hue everywhere exceeding three units. The centroid of each cooled unit was assumed to be a nucleation site, provided a bubble could be seen close to the site in the upper view of the boiling surface.

This matching of Hue pattern and bubble image was not completely unambiguous for small bubbles because of small-scale noise in the Hue data, the possibility that a bubble with a lifetime of less than 10 ms might not be illuminated by a single $20 \mu\text{s}$ flash and the uncertainty in determining in the upper view the exact position of the source of a small bubble that might have detached from the surface.

The plot of nucleation sites identified by this procedure, Fig. 9(a), includes a patch of sites associated with very small bubbles (lower right) that were mostly eliminated by the requirement that the bubbles be visible in at least two successive fields, Fig. 9(b). The centroid of larger cooled regions may not coincide exactly with the nucleation site because of the varying asymmetry of the thermal disturbances caused by bubbles (Section 5), so apparent clusters of sites may possibly be a single site. The plot was therefore simplified by consolidating sites lying within 1 mm of each other, giving a total of 48 sites in the area of 2.2 cm^2 . Then, analysis of the video film provided for each site the number of bubbles produced over 12 s, the maximum size of the thermal disturbance (which has been shown in Section 5 to correspond closely to the maximum bubble size) and the wall temperature-time history at the site. The sites were divided into three groups: those producing 1–4 bubbles, those producing 5–10 bubbles and the most active group producing 17–63 bubbles in 12 s. The sites are shown with their average bubble sizes in Fig. 9(c). It appears that most of the surface is influenced by bubbles. However, the most active sites, including sites A and B examined in Section 5, directly influence only 33% of the surface, Fig. 9(d). Later in this section we shall examine the interactions between site A and its adjacent sites shown in Fig. 9(e), using their temperature-time histories.

The histories for sites A and B over 12 s are shown in Fig. 10 with marks for bubble nucleation events, including those analysed in detail in Section 5. They show repeated, but irregular, patterns of rapid cooling following nucleation, then more gradual recovery of temperature until the next bubble nucleates. Sometimes cooling occurs without nucleation, caused by bubble growth at an adjacent site, and sometimes there are unusually prolonged recovery periods. These

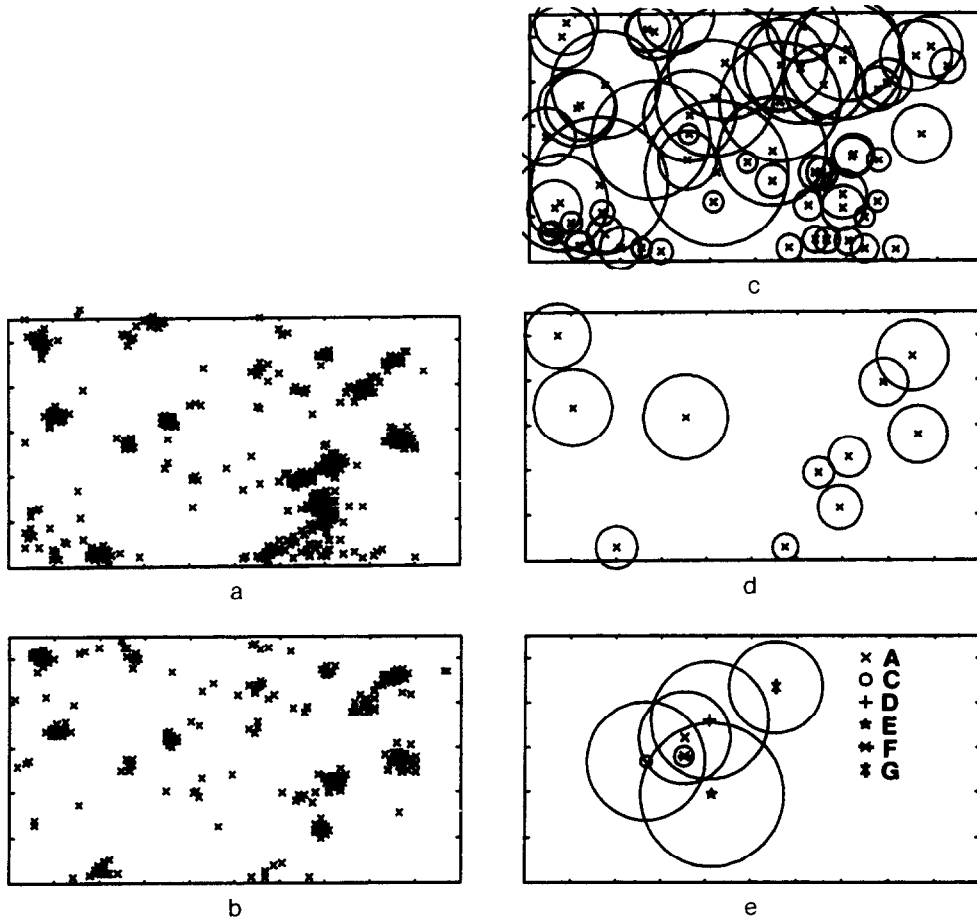


Fig. 9. (a) Bubble centres, 12 s period at 50.8 kW m^{-2} , (b) bubble sites, bubble lifetimes $\geq 20 \text{ ms}$, (c) consolidated bubble sites and average maximum bubble size, (d) most active sites (17–63 bubbles in 12 s), (e) site A and interacting sites C, D, E.

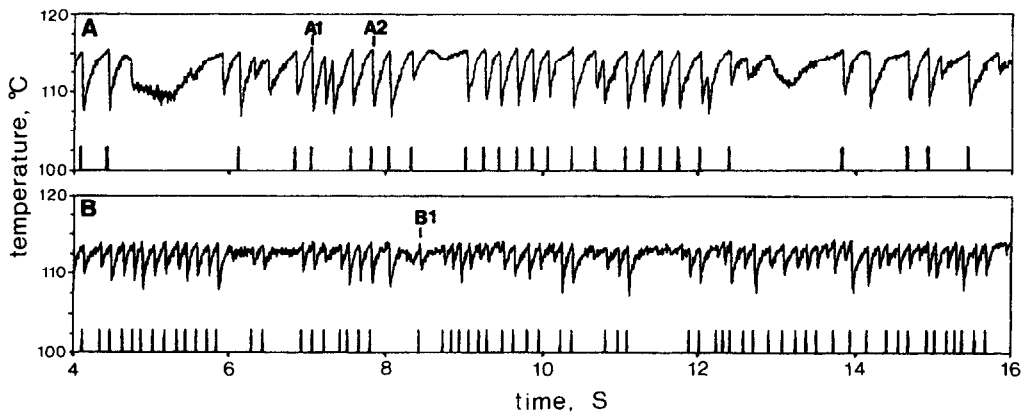


Fig. 10. Temperature-time histories, A site A, B site B.

sites were typical of all the sites, in that nucleation occurred at a local superheat that was constant for a given site within $\pm 0.3 \text{ K}$, i.e. within the signal noise. The number distributions of the three classes of sites (1–4, 5–10, 17–63) against wall superheat for

nucleation are shown in Fig. 11. The average wall superheat is 13.7 K . The most active group of sites have nucleation superheats in the range $8.4\text{--}15.5 \text{ K}$ (effective radii of $3.4\text{--}1.6 \text{ microns}$), distributed throughout the range. The less active sites are dis-

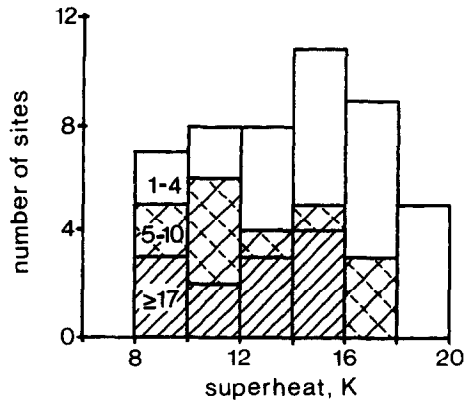


Fig. 11. Number distribution of sites against nucleation superheat.

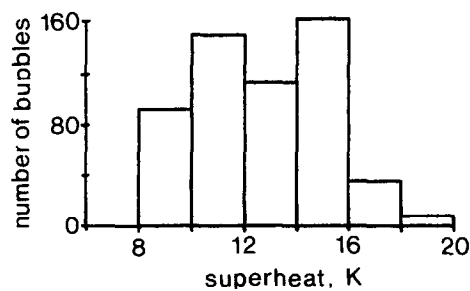


Fig. 12. Number distribution of bubbles against nucleation superheat.

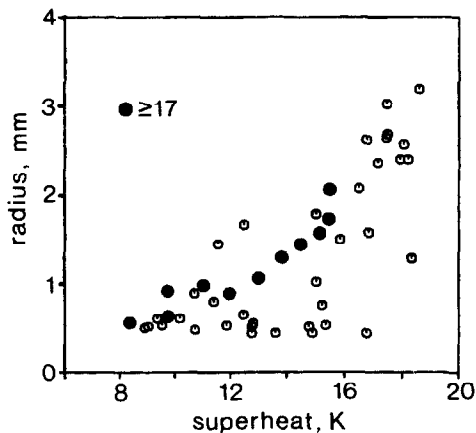


Fig. 13. Average maximum bubble radius against nucleation superheat.

tributed across the range of superheats from 8.9 to 18.6 K. Sites with nucleation superheats exceeding 16 K do not contribute much to the total number of bubbles produced, Fig. 12, but we shall show later that they can influence the productivity of sites active at lower superheats. For the most active group of sites, the maximum bubble radius correlates with the nucleation superheat, Fig. 13: some scatter is to be expected because of the variations in wall superheat around sites, described in Section 5. Consequently the production of bubbles specified by vapour volume, a

measure of the heat transferred by microlayer evaporation, will be biased towards higher superheats, compared to Fig. 12, but we do not have sufficiently accurate values of bubble departure volumes to be able to calculate the distribution.

Next we examine some of the irregularities in bubble production at site A, which is overlapped by bubbles produced at sites C, D and (just) E and lies just beyond the perimeters of bubbles produced at sites F and G, Fig. 9(e). Combined temperature-time histories over 6 s for sites A, C, D and E are shown in Fig. 14(a). Site A nucleates when its temperature reaches 115.5°C, site C at 117.4°C, site D at 116.8°C and site E at 118.6°C. Every time a bubble nucleates at C, causing a temperature drop of about 8 K at its own site, it causes a small temperature drop of about 4 K at site A, as marked on Fig. 14(a). The reciprocal cooling of site C by bubbles nucleating at A is only 1 or 2 K because the bubbles from site A are smaller and only just reach C. Sites D and E each produce only one bubble during the period covered by Fig. 14(a). The bubble from D causes cooling by 6 K at A, while the bubble from E only just reaches A and its effect is hardly discernable. The complexity that can occur in the interactions between sites is illustrated by the events immediately following the nucleation of bubble A1 at 07:050, Fig. 14(a). The resulting small cooling at C occurs just as C is about to nucleate so nucleation is delayed until after a short recovery period. The bubble C1 then produces a strong cooling effect at A, interrupting the recovery of superheat following bubble A1. This removes the cooling effect that A normally exerts on site D, so that D can produce a bubble. This bubble cools A, interrupting the second recovery period after bubble A1, so that A is deactivated for two cycles by the combined effects of C and D. Then the temperature at A recovers more rapidly than at C and D, reactivating A for four bubble cycles up to bubble A3 at 08:300. These bubbles at A keep C and D below their nucleation temperatures. Bubble A3 nucleates at the normal temperature for site A, but is unusually small, causing only half the usual local cooling. There is no bubble activity at immediately adjacent sites to cause this anomaly, but the wall superheat around A is lower than usual, which would reduce the later stages of microlayer evaporation. Following A3, the wall temperature recovers to the nucleation temperature for A, but no bubble is produced: instead the temperature falls gradually before rising again to the nucleation temperature, this time with bubble production at 09:050. This period of inactivity appears to be caused by unusually large convective cooling by the subcooled bulk liquid affecting the region of sites A, C and D, but not the entire boiling surface. Similar periods of inactivity occur at times in all the site temperature-time histories. The interruptions in bubble production appear to be caused by a combination of these fluctuations in convection and the interactions with other sites. For sites that produce many sites during a period of obser-

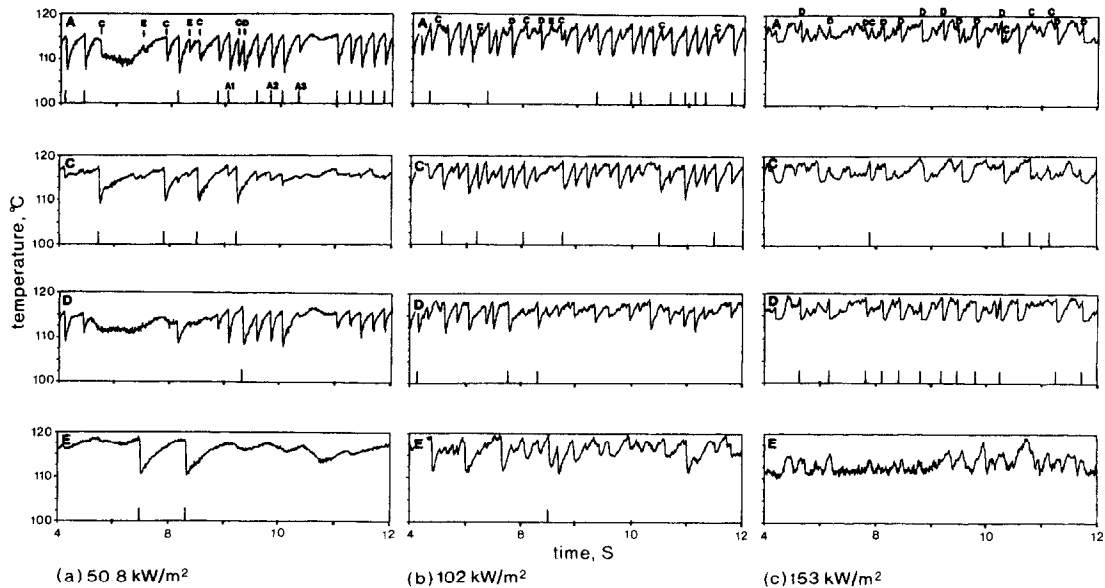


Fig. 14. Interactions between sites A, C, D, E at (a) 50.8 kW m^{-2} , (b) 102 kW m^{-2} , (c) 153 kW m^{-2} .

vation an 'intermittency factor' can be defined by the ratio of the smallest period between bubbles to the mean period: site A has an intermittency factor of 0.5 and site B, a very active site, has a factor of 0.7. However, this definition is unworkable for sites that produce very few bubbles.

All the data discussed so far were obtained at the lowest heat flux of 50.8 kW m^{-2} . Because the identification of all sites and examination of their interactions are so time-consuming, the analysis has not yet been completed for higher heat fluxes. Preliminary trials have shown that a more sophisticated image-analysis routine is required that can distinguish overlapping patterns of Hue round closely spaced sites. The detection of bubbles in the upper view of the surface becomes less reliable because of obstruction by other bubbles. For this paper we have performed a limited analysis of the temperature-time histories at the sites A, C, D, E and their interactions at heat fluxes of 102 and 153 kW m^{-2} , Fig. 14(b, c). At 102 kW m^{-2} the sites nucleate at nearly constant superheats that are higher than those required for nucleation at 50.8 kW m^{-2} by amounts ranging from 2.3 K for site A to 0.8 K for site E, Table 1. Site A produces bubbles of nearly the same size and at nearly the same average rate as it did at the lower heat flux, but now its intermittency is caused mainly by the much-increased activity at sites C and D, with little evidence of suppression by periods of unusually high convective cooling at A, Fig. 14(b). At 153 kW m^{-2} site A is inactive, even though the local superheat reaches 19.5 K , 4 K more than the superheat required for sustained activity at 50.8 kW m^{-2} . Site E is inactive because of a general reduction in its local superheat by other bubbles and by convective cooling spreading inwards from the edge of the plate. There are further small increases in the nucleation superheats at sites C

and D, Table 1. Site C decreases in activity, but site D increases its rate of production of bubbles. There is a change in the character of the temperature-time histories at the active sites (particularly site D) immediately following bubble growth: there is now a delay of $50\text{--}100 \text{ ms}$ before recovery of superheat commences, Fig. 14(c), whereas at lower heat fluxes recovery started almost immediately. This phenomenon is under further investigation.

At a given heat flux, each site has a characteristic nucleation superheat which varies about its mean value by amounts that are only slightly greater than the noise in the measurement of temperature. Therefore it is not possible to relate these variations to the small variations in the minimum wall superheat immediately preceding nucleation, or the variations in convective cooling by the bulk liquid at the instant of nucleation, but any effects must be small. Increasing the heat flux from 50.8 kW m^{-2} to 153 kW m^{-2} increases the nucleation superheats at sites A, C, D, by 3.6 , 1.2 and 1.8 K , respectively, if full allowance $q_0 \delta / 2k$, is made for the steady-conduction temperature difference across the wall. The effective radii calculated from the nucleation superheats at 50.8 kW m^{-2} for A, C, D, are 1.62 , 1.38 and 1.43 microns , respectively. At first sight the increases in nucleation superheats with increasing heat flux are consistent with the Hsu [18] or Bergles-Rohsenow [19] models for the effect of the temperature gradient in the liquid round a site. The Hsu model assumes transient conduction in the liquid, whereas we have shown in Section 5 that convective cooling is established before nucleation. The Bergles-Rohsenow model assumes convective cooling, but the predicted effect is very small for the sizes of cavities active in these experiments: for a heat flux of 153 kW m^{-2} into the liquid the temperature difference across a nucleus protruding

Table 1. Nucleation superheats

Site	Heat flux kW m ⁻²	ΔT nucleation K (average)	Preceding ΔT K (max) (min)		Wall ΔT $q \delta / 2k$	ΔT nucleation K (corrected)
A	53	15.5	7.0	9.9	-0.2	15.3
	102	17.8	8.8	11.5	-0.4	17.4
	153	> 19.5	inactive		-0.6	> 18.9
C	50	17.4	9.0	9.7	-0.2	17.2
	102	18.4	10.1	12.4	-0.4	18.0
	153	19.0	14.0	14.7	-0.6	18.4
D	50	16.8	8.8	8.8	-0.2	16.6
	102	18.0	11.5	13.5	-0.4	17.6
	153	19.0	13.8	14.2	-0.6	18.4
E	50	18.6			-0.2	18.4
	102	19.6	11.2	11.2	-0.4	19.2
	153	inactive			—	—

1.6 microns from the wall is only 0.4 K. The increases in nucleation superheat are accompanied by increases in the minimum superheat preceding nucleation, Table 1, so they cannot be caused by increased penetration of liquid into the cavity during the cooling phase of the bubble cycle [20], unless there is a marked decrease in contact angle in the temperature range 108–120°C. A possible explanation of the increase lies in the effect of dissolved air in these experiments in an open tank. At the lowest heat flux the bulk liquid was subcooled. Although some bubbles reached the free surface, stripping air from the liquid, they also promoted a vigorous circulation of the liquid, which would have reabsorbed and redistributed some air. With increasing heat flux the bulk subcooling decreased and the removal of dissolved air would have increased. A concentration of 20% of equilibrium dissolved air (partial pressure 20 kPa) at the lowest heat flux decreasing to near-zero at the highest flux would be sufficient to explain the behaviour of site A; the smaller effects at sites C and D might depend on rates of mass transfer of dissolved gas within cavities. The number of sites examined here is too small to draw firm conclusions and the study must be extended to all the active sites: the difficulties in so doing have been noted above. The observations draw attention to the necessity for better control of bulk temperature and dissolved gas in future experiments. We have shown that the Hsu [18] and Bergles-Rohsenow [19] nucleation models are not relevant for the conditions of the present experiments. In conditions in which they might be applicable, e.g. at higher heat fluxes and/or with larger active cavities, we note that it would be essential to use local values of wall superheat and heat flux into the liquid, not average values as is customary.

The ability of sites to survive temporary reductions in superheat to about half the nucleation superheat, doubling the equilibrium radius of curvature of the nucleus, indicates that the nucleus must be pinned at

a sharp geometrical discontinuity, either at the mouth of the cavity or deeper inside [20], or at a discontinuity in wettability within the cavity [21]. Wettability can only be observed on the wall outside the cavities. The reduction in the number of cavities active at low superheats after the cleaning that produced the well-wetted condition with a contact angle of less than 20° indicates that the cleaning process penetrated many cavities. Supposing that the remaining active cavities had internal contact angles of 20°, stability against the observed reductions in superheat would require a re-entrant geometry with a half-angle of at least 40°. Alternatively a local increase in contact angle to 60°, approximately the external value before cleaning, in a cylindrical region of a cavity would be just sufficient to ensure stability, Fig. 15. We do not know which mechanism produced the stable sites in this study. A dependence on internal variations in contact angle and therefore, on the efficiency of the cleaning process, would introduce variability into boiling experiments that could not be controlled by measurements of surface microgeometry and external contact angle alone. The difficulty of specifying uniformity of wetting conditions within all cavities may affect any experiment

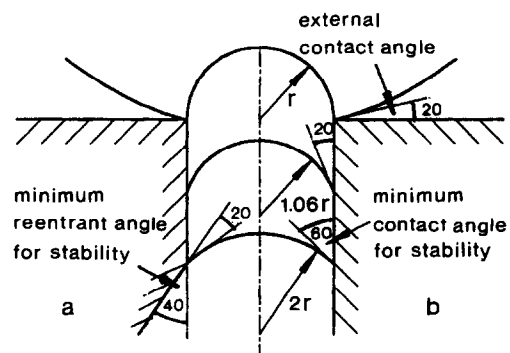


Fig. 15. Stabilization of nucleation site by (a) geometry, (b) change in contact angle.

in which contact angle is modified by surface treatment, e.g. by controlled oxidation [22].

Whatever the conditions that determine the nucleation superheat and stability of a cavity, each active site in this study has a nucleation superheat that is constant when boiling at a steady input heat flux and which sets a maximum value for the wall superheat at the site. The growth of a bubble cools a surrounding 'area of influence' equal to the maximum size of the bubble. The distribution of temperature over this area is not necessarily symmetrical, Fig. 7, because some regions may fall within the areas of influence of several active sites and are also subject to fluctuations in the convective cooling driven by the collective motion of bubbles: this introduces variability into the size of bubbles produced by a site. Active sites can co-exist within one bubble radius of each other, in contrast to the inhibition within two bubble radii reported by Del Valle and Kenning [17] for highly subcooled flow boiling. The sites then interact through the variations in wall temperature that each produces, introducing intermittency in the regular production of bubbles, as illustrated by the group of sites A, C, D, E, in Fig. 14. The primary interactions limited to a range of one bubble radius may be extended to greater distances by chain interactions between several sites. Lateral conduction in the wall, which would also extend the range of the interactions, is inhibited by the particular conditions of these experiments. For boiling on a thin wall with long recovery periods of convective cooling between bubbles the fin effect attenuates the temperature variations over a distance of order $(k_s \delta / h)^{1/2}$. For these experiments on 0.13 mm thick stainless steel with $h \sim 2 \text{ kW m}^{-2} \text{ K}^{-1}$, the distance is only 1.0 mm.

The strongest interactions are to be expected between closely-spaced sites with similar nucleation superheats. A site with a high nucleation superheat is likely to be completely deactivated by the cooling effect of an adjacent site with a low nucleation superheat; however, simultaneous activity with interaction is possible if (i) the site of low superheat is intermittently inhibited by the action of a third site or (ii) the site of high superheat produces larger bubbles and is placed at such a distance that it cools the site of low superheat without experiencing reciprocal cooling. All the examples of intermittency in these experiments have involved at least two interacting sites; we have not yet found any examples of gradually self-induced intermittency of the sort postulated by Kenning [1, 20], although many sites produced only one bubble.

In these examples sites have been shown to interact through variations in wall temperature. Judd and Chopra [23] have proposed a different mechanism of interaction which also has a primary range of one bubble radius, which may be extended by chain interactions between several sites. They suppose that growth of a bubble either activates adjacent sites that are poor vapour traps by 'seeding' or deactivates sites by displacing their trapped vapour. Their model is based on observations of saturated boiling of dichloro-

methane on a thick glass wall with a thin coating of stannic oxide. This sort of surface may have a high concentration of shallow, well-wetted cavities that are poor vapour traps, but large variations in local temperature are also to be expected on a wall of such low thermal diffusivity. If seeding requires temporary dryout of the wall, it is unlikely under the conditions of our experiments on stainless steel, since the evidence discussed in Section 5 suggests that most of the wall remains wet during bubble growth and departure.

The spatial and size distributions of the nucleation sites determine the large-scale variations in wall superheat during boiling at constant input heat flux. Spatial distributions of the total populations of active sites, discounting interactions, have been found to be random [17, 24, 25]. There is no information about whether the distributions within narrow size bands are also random: such a study would require experiments with very large populations of sites, larger than in typical laboratory experiments. Randomness appears to be as good a modelling assumption as any, but manufacturing processes of industrial heat transfer surfaces, such as drawing and rolling, might well produce more clustering of similar sites than would occur in a truly random distribution. The variations in wall superheat also depend on whether the nucleation superheat of an active site always places an upper limit on the local wall superheat, as it has in these experiments. The growth of a bubble must always produce some local cooling. The rate of recovery to the nucleation superheat determines the waiting period between bubbles and depends on the thermal diffusivity of the wall and the input heat flux. Reducing the waiting period will eventually lead to recovery to the nucleation superheat while the nucleation site is dry, either through dryout of the microlayer and recovery of the superheat before the liquid returns or through interference between successive bubbles creating a vapour column. Either process will invalidate the quasi-static model that links the wall superheat to the critical radius of a cavity: the local maximum wall superheat will then depend on dynamic processes.

The experimental observations reported in this paper reveal rich sources of variability in pool nucleate boiling, all interacting strongly with local variations in wall superheat. These essential phenomena cannot be modelled by the approach exemplified by Mikic and Rohsenow [11], in which a uniform (or average) wall superheat is combined with a specification of the size distribution of wall cavities to predict a population of active nucleation sites that increases smoothly by the addition of extra sites at higher heat fluxes, and in which each active site makes the same steady contribution to bubble production. We have given examples of the deactivation of sites and exchange of activity between sites with increasing heat flux, similar to the previously reported behaviour in subcooled flow boiling [17], although not necessarily for exactly the same reasons, and we have shown that

intermittency has a big effect on the bubble production at different sites. The observations provide strong support for the modelling approach developed by workers at the Los Alamos National Laboratory [6, 7] in which large-scale computational 'experiments' explore the interactions between many nucleation sites through the variations in wall superheat. Their studies address important questions about the measurement of wall superheat that were discussed in a less sophisticated way in the earlier account of pool boiling experiments with liquid crystals [1]. We can expect that the representations of the local physics of boiling in such models will be gradually improved. This may not necessarily lead to a general improvement in the accuracy of predictions of boiling heat transfer if the requisite specifications of surface conditions of microgeometry and microwettability cannot be provided for all situations. At least the models will provide a proper appreciation of the uncertainty in translating data from laboratory experiments into design data for industrial heat exchangers.

7. CONCLUSIONS

Pool boiling of water on a thin, electrically-heated stainless steel plate in an open tank has been investigated by liquid-crystal thermography in combination with high-speed video recording. These preliminary experiments show that the limitations of the technique in respect of accuracy and frequency response are outweighed by its unique capacity to measure wall temperature variations with high spatial resolution over an area encompassing many nucleation sites and over long periods. The experimental and analytical methods are capable of further improvement. The technique is necessarily limited to boiling on a thin wall, which accentuates the variations in wall temperature, so caution is required in extrapolating the observations to other conditions. The effects of wall thickness and thermal properties should be examined by numerical modelling.

The measurements confirm the importance of variations in wall temperature for the removal of heat by bubbles and the activity of nucleation sites. Models that assume uniform wall temperature cannot represent the fundamental physics of boiling.

The nature of the wall temperature variations is sensitive to the wettability of the heated surface. The following observations refer to water boiling at low heat fluxes on a well-wetted surface, although the external observation of contact angle may not apply to conditions within the active nucleation sites.

The cooling of the wall during bubble growth is consistent with evaporation of a liquid microlayer, but further investigation is required of the state of the microlayer close to the nucleation site. Evaporation of the microlayer is affected by the spatial distribution of wall superheat at the instant of nucleation; the distribution is dependent on the growth of preceding bubbles at the site and at adjacent sites, and may

therefore be asymmetrical. There is further cooling during the contraction of the base of the bubble up to the instant of detachment. This cooling is less than that predicted by a model of uniform quenching by transient conduction into stagnant liquid at the bulk temperature. Throughout the growth and departure of a bubble its direct cooling effect is confined to its maximum contact area with the wall. The radius of the 'area of influence' is equal to the maximum bubble radius and the cooling decreases near the outer edge of this area.

Following bubble departure, the wall superheat recovers at a rate dependent on the imbalance between the electrical heat input and the local convective cooling, which is rather more than twice the cooling expected for single-phase natural convection. The convective cooling fluctuates, but there is no pattern that can be identified with the wake of a particular rising bubble.

At a given heat flux, each nucleation site has a characteristic nucleation superheat. Nucleation occurs when the local wall superheat recovers to this critical value. For the limited number of sites so far examined, the nucleation superheats increase with increasing heat flux by amounts that are too large to be explained by conventional models for the effect of the temperature gradient in the liquid around a nucleus. The increases may be consequences of changes in bulk subcooling and dissolved gas content, which were insufficiently controlled during these experiments in an open tank.

Nucleation sites located within one bubble radius of each other interact through the fluctuations in wall temperature caused by bubble growth. Sites with high nucleation superheats tend to produce larger bubbles than sites with smaller nucleation superheats, so a site of high superheat can influence a site of low superheat without being subjected to a reciprocal effect. The range of influence of a site can be increased beyond one bubble radius by chain interactions among a group of sites. The range could also be increased by lateral conduction in a thicker wall of higher conductivity than was used in these experiments.

The interactions between sites cause intermittency that has a large effect on the net rate of bubble production at individual sites. Increases in heat flux activate some new sites, but also increase the activity at some existing sites and decrease the activity at others. This sort of behaviour cannot be represented by models that assume uniform wall superheat and constant rates of bubble production at uniform size and frequency at all active sites.

Intermittency is also caused by the fluctuations in convective cooling by the bulk liquid. At low heat flux the fluctuations occur over relatively small regions, perhaps through the combined effects of groups of bubbles. At high heat flux the bubble-driven circulation in the tank causes more regular, but pulsating, convective cooling, spreading inwards from the edges of the test section.

The modelling of nucleate boiling must take account of the variations in wall temperature, which have important implications for the way experimental boiling data should be obtained and interpreted. The way to a better understanding of boiling may lie in a combination of experiments such as those described here with very large-scale numerical calculational 'experiments' of the sort described by other workers [6, 7].

Acknowledgements—This work was supported by the Engineering and Physical Sciences Research Council under grant no. GR/H45377. Professor H. J. Coles of Southampton University generously provided samples of liquid crystal.

REFERENCES

1. D. B. R. Kenning, Wall temperature patterns in nucleate boiling, *Int. J. Heat Mass Transfer* **35**, 73–86 (1992).
2. D. B. R. Kenning, Pool boiling on a thin horizontal plate, Video Film, Oxford University Department of Engineering Science (1991).
3. D. B. R. Kenning, Liquid crystal thermography as a tool for investigating the development of boiling, *Proceedings of the Engineering Foundation Conference on Pool and External Flow Boiling*, Santa Barbara, pp. 79–82 (1992).
4. W. Bergez, Nucleate boiling on a thin plate: heat transfer and bubbling activity of nucleation sites, *Int. J. Heat Mass Transfer*, **38**, 1799–1811 (1995).
5. Youyou Yan and D. B. R. Kenning, Liquid crystal measurements of wall temperatures in boiling heat transfer, *Proceedings of the Seminar on Optical Methods and Data Processing in Heat and Fluid Flow*, I. Mech. E. London, pp. 49–58 (1994).
6. K. O. Pasamehmetoglu and R. A. Nelson, Cavity-to-cavity interaction in nucleate boiling: the effect of heat conduction within the heater, *A.I.Ch.E. Symp. Ser.* **282**(87), 342–351 (1991).
7. P. Sadasivan, C. Unal and R. A. Nelson, Nonlinear aspects of high heat flux nucleate boiling heat transfer, Parts I and II, ASME Winter Meeting, Chicago (1994).
8. F. D. Moore and R. B. Mesler, The measurement of rapid surface temperature fluctuations during nucleate boiling of water, *A.I.Ch.E. J.* **7**, 620–624 (1961).
9. M. G. Cooper and A. J. P. Lloyd, Transient local heat flux in nucleate boiling, *Proceedings of the third International Heat Transfer Conference*, Chicago, Vol. 1, pp. 193–198 (1966).
10. M. G. Cooper and T. T. Chandratilleke, Growth of diffusion-controlled vapour bubbles at a wall in a known temperature gradient, *Int. J. Heat Mass Transfer* **24**, 1475–1492 (1981).
11. B. B. Mikic and W. M. Rohsenow, A new correlation of pool boiling data including the effect of heating surface characteristics, *ASME J. Heat Transfer* **91**, 245–250 (1969).
12. M. G. Cooper and A. J. P. Lloyd, The microlayer in nucleate pool boiling, *Int. J. Heat Mass Transfer* **12**, 895–913 (1969).
13. D. A. Spence and D. B. R. Kenning, Unsteady heat conduction in a quarter plane, with an application to bubble growth models, *Int. J. Heat Mass Transfer* **21**, 719–724 (1978).
14. P. C. Wayner, Evaporation and stress in the contact line region, *Proceedings of the Engineering Foundation Conference on Pool and External Flow Boiling*, Santa Barbara, pp. 251–256 (1992).
15. P. S. Roberts, The influence of wall thermal properties on bubble dynamics and heat transfer in nucleate boiling, D. Phil. thesis, Oxford University Department of Engineering Science (1984).
16. R. L. Judd and C. H. Lavdas, The nature of nucleation site interaction, *ASME J. Heat Transfer* **102**, 461–464 (1980).
17. V. H. del Valle and D. B. R. Kenning, Subcooled flow boiling at high heat flux, *Int. J. Heat Mass Transfer* **28**, 1907–1920 (1985).
18. Y. Y. Hsu, On the size range of active nucleation cavities on a heating surface, *ASME J. Heat Transfer* **84**, 207–216 (1962).
19. A. E. Bergles and W. M. Rohsenow, The determination of forced-convection surface-boiling heat transfer, *ASME J. Heat Transfer* **86**, 365–372 (1964).
20. D. B. R. Kenning, Wall temperature variations and the modelling of bubble nucleation sites, *Proceedings of the Engineering Foundation Conference on Pool and External Flow Boiling*, Santa Barbara, pp. 105–110 (1992).
21. K. Cornwell, On boiling incipience due to contact angle hysteresis, *Int. J. Heat Mass Transfer* **25**, 205–211 (1982).
22. C. H. Wang and V. K. Dhir, On the prediction of active nucleation sites including the effect of surface wettability, *Proceedings of the Engineering Foundation Conference on Pool and External Flow Boiling*, Santa Barbara, pp. 111–118 (1992).
23. R. L. Judd and A. Chopra, Interaction of the nucleation processes occurring at adjacent nucleation sites, *ASME J. Heat Transfer* **115**, 955–962 (1993).
24. R. F. Gaertner, Distribution of active sites in the nucleate boiling of liquids, *A.I.Ch.E. Symp. Ser.* **41**(59), 52–61 (1963).
25. M. Sultan and R. L. Judd, Spatial distribution of active sites and bubble flux density, *ASME J. Heat Transfer* **100**, 56–62 (1978).
26. H. S. Carslaw and J. C. Jaeger, *Conduction of Heat in Solids* (2nd Edn). Clarendon Press, Oxford (1959).

APPENDIX A

The one-dimensional quenching model assumes that, as a bubble lifts off, the wall is brought into instantaneous contact with semi-infinite liquid which is initially at its bulk temperature, $T_1 = T_b = 0$ say, everywhere except at the contact with the wall which is at an initial temperature $T = T_0$ at $z = 0$, $t = 0$. Heat is then conducted into stationary liquid so that

$$\frac{\partial T_1}{\partial t} = \alpha_1 \frac{\partial^2 T_1}{\partial z^2} \quad (\text{A1})$$

and the temperature of the thin wall is given by

$$\rho_s c_s \delta \frac{\partial T}{\partial t} = q_0 + k_1 \left(\frac{\partial T_1}{\partial z} \right)_{z=0} \quad (\text{A2})$$

The solution for $T(t)$ is the sum of the solutions given in ref. [26] for $T_0 \neq 0$, $q_0 = 0$ and $T_0 = 0$, $q_0 \neq 0$:

$$T = \left(T_0 + \frac{q_0}{k_1 b} \right) \exp(bx + b^2 \alpha_1 t) \operatorname{erfc} \left(\frac{x}{2\sqrt{\alpha_1 t}} + b\sqrt{\alpha_1 t} \right) + \frac{2q_0}{k_1} \sqrt{\frac{\alpha_1 t}{\pi}} \exp\left(\frac{-x^2}{4\alpha_1 t}\right) - \frac{q_0(1+bx)}{k_1 b} \operatorname{erfc} \left(\frac{x}{2\sqrt{\alpha_1 t}} \right), \quad (\text{A3})$$

where

$$b = \frac{\rho_1 c_1}{\rho_s c_s \delta} \quad (\text{A4})$$

The model is compared with the measured wall temperature variation at the centre of bubble A1, described in Section 5, Figs 7, 10. The instant of lift-off is some time between 07:065 and 07:070, so the measured conditions at

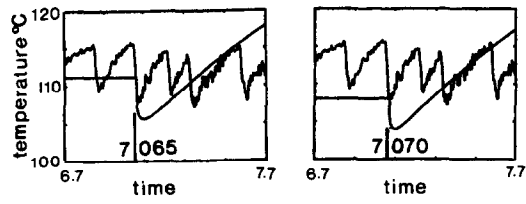


Fig. A1. Comparison of wall quenching model with data.

these times are taken as the initial conditions, Fig. A1. The model predicts a larger initial dip in temperature and larger rates of cooling during the recovery period than are observed experimentally. Even larger rates would be predicted near the periphery of the bubble because of the higher initial wall temperature there. The quenching model, even if confined to the bubble contact area, greatly overestimates the heat transfer to the bulk liquid following bubble departure under these conditions.